Optica Applicata, Vol. XLII, No. 4, 2012
DOI: 10.5277/oa120421

A high sensitivity vector accelerometer based on tri-axial fiber Bragg grating

QI JIANG*, MENG YANG

School of Control Science and Engineering, Shandong University,
73 Jingshi Road, Jinan, Shandong 250061, China

*Corresponding author: jiangqi@sdu.edu.cn

Firstly, a single-axis FBG accelerometer with intensity modulation-direct detection interrogation system was put forward and designed in the paper. Experiments with different excitation frequencies were implemented, which demonstrate its good mechanical structure and fabrication technology. Accordingly, a novel tri-axis FBG accelerometer based on the single-axis FBG accelerometer was proposed and a series of periodic vibration tests were finished to prove its performance at different excitation frequencies. The response of the tri-axis vector FBG accelerometer can keep up with the increasing excitation frequency with good signal-to-noise ratio (SNR) within 160 Hz. The suitable measurement frequency range of the accelerator is between 0 and 500 Hz. The cross-axis response among three axes is analyzed. These experiments indicate that horizontal axes have less influence on the vertical axis vibration of FBG.

Keywords: three axes, fiber Bragg grating, accelerometer.

1. Introduction

Vibration measurement is a critical issue in modern engineering application. Accelerometers play an important role in practical applications, such as structural--health monitoring, earthquake, *etc*. [1–3]. Over the last two decades, fiber Bragg grating (FBG) based sensors have brought a great attention to researchers and engineers. Numerous advantages have been discovered as well [4, 5].

Many new designs of accelerometer based FBG have been proposed and the physical structures of the transducers vary significantly from one type to another [6–12]. Due to the distinguished features of the mechanical transducer designs, the existing FBG based accelerometers can be described in two categories: those in which the proof mass is part of a cantilever structure whose deflection can be sensed optically. And those in which a fiber is strained by motion of the proof mass. As examples of the former, a L-shaped rigid cantilever beam, a concentrated mass, a leaf spring and a FBG element were used to detect strains due to imposed acceleration in [8]. A FBG-based accelerometer designed from a dual flexural beam approach was presented in [9]. The mechanism of other sensor functions by a coupling between

an inertial mass vibration and the induced strain within FBG. An accelerometer based on a single degree-of-freedom system was presented in [10]. A mass resting on a layer of compliant material was supported by a rigid base plate. An accelerometer based on two FBGs in opposite positions was proposed in [11]. The accelerometer is manufactured from a bulk brass piece and its structure consists of a concentrated inertial mass, supported by a L-shaped cantilever beam, connected to the base by a thin element (with a thickness of 1.1 mm) and by two Bragg grating elements.

Good features had been achieved by many single-axis and double-axis FBG accelerometers. However, a multiple-axis FBG accelerometer to detect the 3D acceleration is less investigated. A tri-axial FBG accelerometer has been designed [13] and realized by mounting three modules [14]. The prototype was accomplished by multiplexing three unidirectional sensing elements, which are fixed along three orthogonal directions x, y and z [13, 15]. Only one axis was inscribed with FBG and experimented in [13]. The relationship among axes was not researched. Multiple masses cannot ensure the frequency measure simultaneously. In this paper, we focus on the application of FBG based accelerometer in shockwave monitoring and the detection of the earthquake. A three-axis FBG accelerometer was proposed, which consisted of three pairs of FBGs and a common mass. Compared with the FBG accelerometers employing glued or embedded FBG in various transducer arrangements, the proposed accelerometer utilized fiber Bragg grating as a spring element, the physical deformation of the FBG elements is the actual mass displacement, and the efficiency of the mechanical energy transfer between the imposed acceleration and FBG strain change is high. So a more accurate method for measurement was realized.

2. FBG-based accelerometer

The elementary fiber Bragg grating comprises a short section of a single-mode optical fiber in which the core refractive index is modulated periodically. The sensing function of an FBG derives from the sensitivity of both the refractive index and grating period to externally applied mechanical or thermal perturbations. The strain field affects the response of an FBG directly, through the expansion and compression of grating pitch size and through the strain-optic effect, that is, the strain-induced modification of the refractive index. The temperature sensitivity of an FBG occurs principally through the effect on the induced refractive index change and, to a lesser extent, on the thermal expansion coefficient of the fiber. Thus, the peak reflected wavelength shifts by an amount $\Delta\lambda_B$ in response to strain ε and temperature change ΔT as given by

$$\frac{\Delta\lambda_B}{\lambda_B} = P_e\varepsilon + \left[P_e(\alpha_s - \alpha_f) + \varsigma\right]\Delta T \tag{1}$$

where λ_B is the wavelength of the peak reflectivity, P_e is the strain-optic coefficient, α_s and α_f are the thermal expansion coefficients of any fiber bonding material and of the fiber itself, respectively, and ς is the thermo-optic coefficient [16].

The normalized strain response at constant temperature is found to be

$$\frac{1}{\lambda_B}\frac{\Delta\lambda_B}{\Delta\varepsilon} = 0.78 \times 10^{-6-1} \tag{2}$$

The normalized thermal response at constant strain is

$$\frac{1}{\lambda_B}\frac{\Delta\lambda_B}{\Delta T} = 6.678 \times 10^{-6}\ ^{\circ}\mathrm{C}^{-1} \tag{3}$$

For grating produced in silica fiber, representative values of the strain- and temperature-induced wavelength shifts are 1 pm/ε and ~10 pm/°C at 1300 nm, respectively.

The FBG accelerometer described here is based on a three degree-of-freedom system. The transducer consists of a seismic mass (aluminium), a rigid frame (carbon steel) and three pairs of FBGs. The actual seismic mass has three holes orthogonally embedded and supposed by three fibers through these holes. The two ends of each optical fiber are fixed at the opposite sidewalls of the rigid frame along three orthogonal directions x, y and z, respectively. The seismic mass is placed at the center of the structure. As shown in the diagram (Fig. 1), optical fibers with FBGs are used as spring

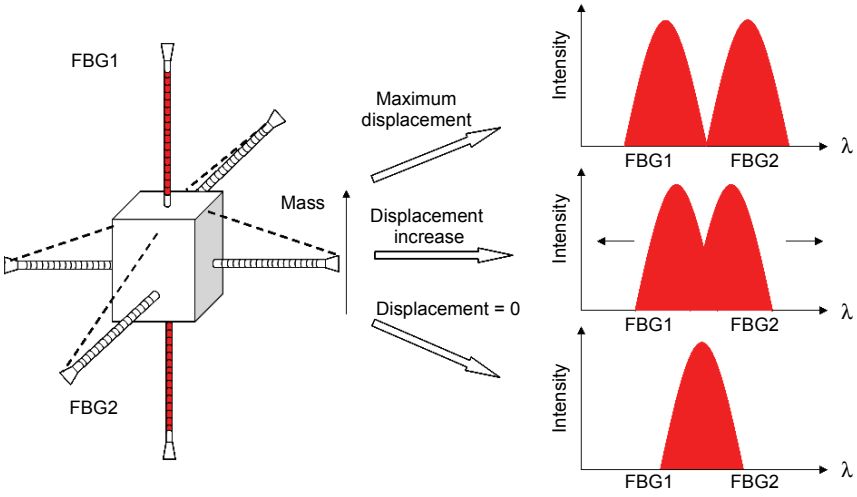

Fig. 1. Acceleration induced Bragg wavelength shifts.

elements. When the transducer is subjected to acceleration vertically, the inertial force of mass results in compression (or elongation) on the upper FBG element and elongation (or compression) on the lower FBG element. The FBG elements will undergo variations in strain as determined by the size of the mass and pretension. The acceleration results in the wavelength-shift response of the fiber Bragg grating. Assuming the transducer undergoes a simple harmonic acceleration of

$$a(t) = \frac{\mathrm{d}^2}{\mathrm{d}t^2} y(t) = A_0 \cos(\omega_0 t) \tag{4}$$

where ω_0 and A_0 are the angular frequency and amplitude of the imposed acceleration.

Then, the overall sensitivity can be expressed as follows:

$$K = 2\left| \frac{-1}{1 - \omega_0 / \omega_n} \frac{1}{\omega_n^2 L_{\mathrm{FBG}}} \right| \quad [\varepsilon/\mathrm{m/s^2}] \tag{5}$$

where L is the effective length of the fiber optic [17].

The resonant frequency of the FBG-based accelerometer can be represented by the expression

$$f_n = \frac{1}{2\pi} \sqrt{\frac{2K_v + 4K_h}{m}} \tag{6}$$

where $K_v = E_1 A/L$ is the spring constant of the fiber optic in vertical direction axis (E_1 is Young's modulus of the fiber, A is the cross-sectional area of the fiber, L is the effective length of the fiber optic), $K_h = 3E_1 I/L^3$ ($I = \pi r^4/4$ is the spring constant of the fiber optic constant in cross-axis), and m is the mass, r is fiber optic's radius. The dimensions of the implemented unit are displayed in Table 1.

Accelerometer induced FBG wavelength changes can be detected by illuminating the FBG with a broadband source. In this paper, FBG central wavelengths were all at 1550 nm without strain. When the transducer is subjected to acceleration vertically, the wavelengths of the vertical pair of FBGs will shift in opposite directions (Fig. 1). The intensity modulation-direct detection (IM-DD) method was introduced for the optical signal interrogation [18]. The light intensity changes proportional to the acceleration can be obtained by a photodetector. On the other hand, the wavelengths of

T a b l e 1. Dimension-related parameters.

	Parameters	Description	Value	Unit
Fiber optic	E_1	Young's modulus of fiber optic	73.1	GPa
	D_1	Signal mode fiber diameter	0.125	mm
	ν	Poisson's ratio	0.17	–
	L_1	Effective fiber length	22.5	mm
Cladding	E_2	Young's modulus of fiber optic	3	GPa
	ν	Poisson's ratio	0.35	–
	D_2	Inner diameter	0.125	mm
	D_3	External diameter	0.25	mm
	L_2	Effective length	22.5	mm
Mass	m	Proof mass	10.0	g
	E_3	Young's modulus of stainless steel	200	GPa
	ν	Poisson's ratio	0.29	–

the horizontal pair of FBGs will shift in the same direction. The intensity reflected by the horizontal pair of FBGs was unchanged.

The temperature compensation is also accomplished by the IM-DD [19]. Any ambient temperature change on the proposed accelerometer would impose the same thermal-optic effect on both of the FBGs, and the two Bragg wavelengths will always shift in the same direction, then the shape of the combined spectrum is not altered, which does not result in light intensity change. However, temperature change will result in the measurement range change.

3. Experiments

After fabrication, the transducer was incorporated into the experimental set-up shown in Fig. 2.

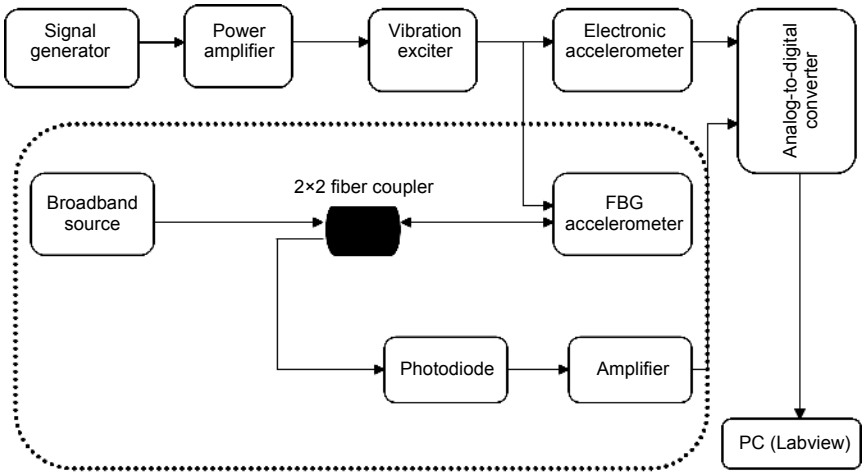

Fig .2. Scheme of the building blocks for the interrogation system.

A broadband light source at 1.5 μm, 20-nm spectral width (FWHM) emitting 21.93 mW light was used to illuminate, through a 2×2 single-mode fiber coupler, the FBG sensor. The reflected signal was guided back through the 2×2 coupler, to the input of InGaAs amplified photodetectors with a responsivity of 0.95 A/W at 1550 nm and a cut-off frequency of 17 MHz.

To characterize frequency response, the FBG accelerometer and a conventional accelerometer were mounted on a shaker. The signal outputs from both the conventional accelerometer and the FBG accelerometer were simultaneously sampled by an analog-to-digital converter, with an input dynamic range of ±5 V and a 16-bit resolution (USB 8361 acquisition board, manufactured by RBH Corporation), and recorded in a laptop by an application implemented in Labview software.

The experimental work for the proposed FBG accelerometer is organized in two major parts: single-axis FBG accelerometer shaking tests and three-axis FBG acceler-

ometer shaking tests. In the first part, a pair of FBG elements was utilized to verify the probability using the IM-DD interrogation method. In the second part, the performance of the three-axis accelerometer was investigated. A number of the issues addressed were discussed in detail.

4. Results and discussion

4.1. Single-axis test

The FBG accelerometer was excited with an electromechanical shaker over a frequency band ranging from 0 to 2500 Hz. The data acquisition was at 5000 samples per second and the sampling number was 10000. The presentations of the signals in time domain and frequency domain are provided in the following figures.

At 5 Hz, the output of the FBG accelerometer in time domain followed the input excitation signals (Fig. 3**a**). The fundamental frequency component was observed

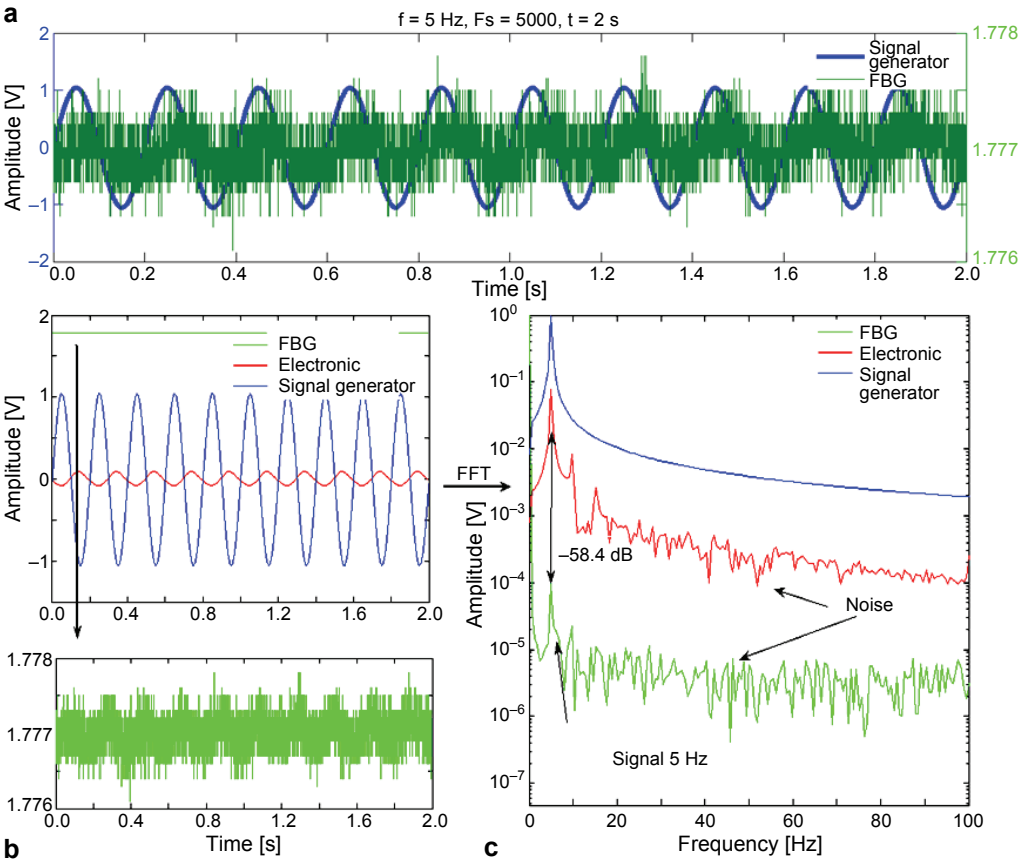

Fig. 3. Input and output signals of the FBG accelerometer at 5 Hz excitation (**a**); input and output signals of accelerometers at 5 Hz excitation (**b**); Fourier transform of input and output signals at 5 Hz excitation (**c**).

at 5 Hz. Harmonics were observed in both the FBG accelerometer and the electronic accelerometer (Fig. 3**c**). Noise was observed at the output of both accelerometers, which was due to the non-uniform response of the exciter at low frequency regions. The output of the FBG accelerometer is approximately 0.0012 times (–58.4 dB above) the electronic accelerometer output (Fig. 3**c**).

At 200 Hz, the output of the accelerometer more closely followed the input excitation signals (Fig. 4**a**). The fundamental frequency component was observed at 200 Hz (Fig. 4**c**).The amplitude of the output signal was found at around 275.1×10^{-5} V, which is higher than 9.411×10^{-5} V at 5 Hz excitation. The output of the FBG accelerometer over the electronic is increased from –58.4 dB to –19.1 dB at 5 Hz, which indicates good sensitivity. A high signal-to-noise ratio was observed. Multiple harmonics were observed as well.

The frequency response of the FBG accelerometer shows similar trends as produced by the electronic accelerometer. This shows that the FBG accelerometer does measure

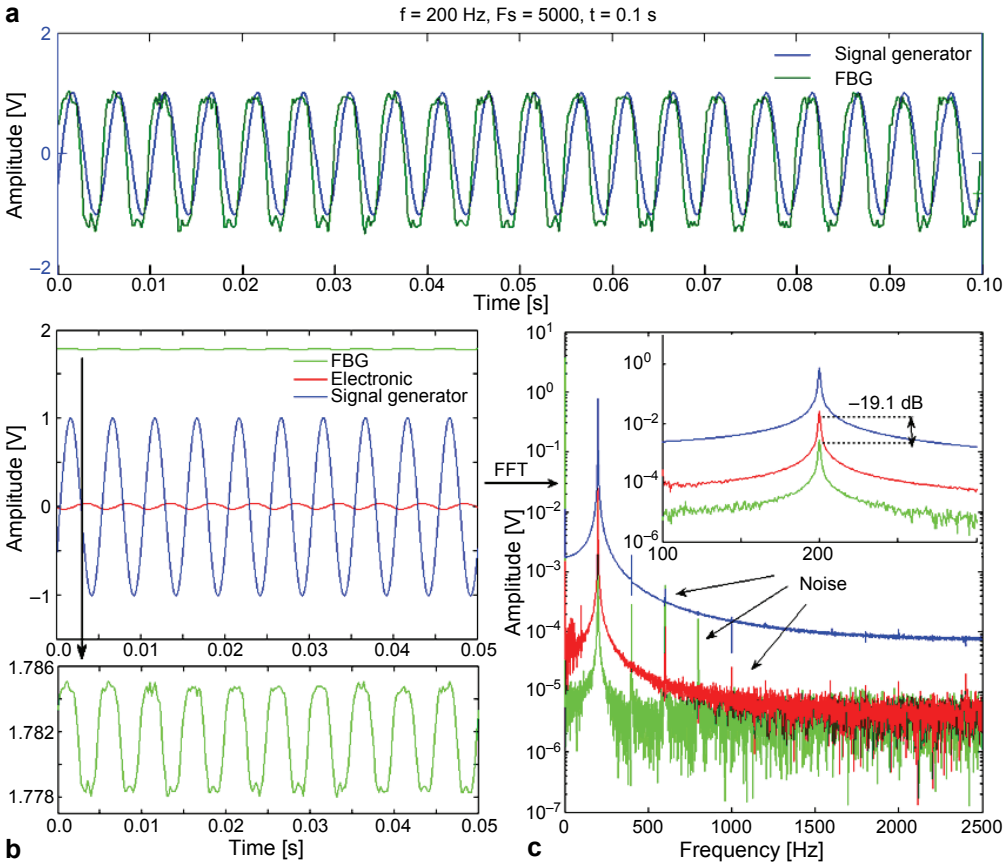

Fig. 4. Input and output signals of the FBG accelerometer at 200 Hz excitation (**a**); input and output signals of accelerometers at 200 Hz excitation (**b**); Fourier transform of input and output signals at 200 Hz excitation (**c**).

the imposed accelerations. The amplitude of the output signal decreased with an increase in the excitation frequency due to the specification of the vibration exciter. Small amplitude was used to achieve a constant displacement of the shaker. A flat region was observed at a lower frequency band, indicating a wide range for measuring acceleration. Figure 5 also shows that the resonant frequency of the FBG accelerometer is 200 Hz, which is higher than the electronic accelerometer.

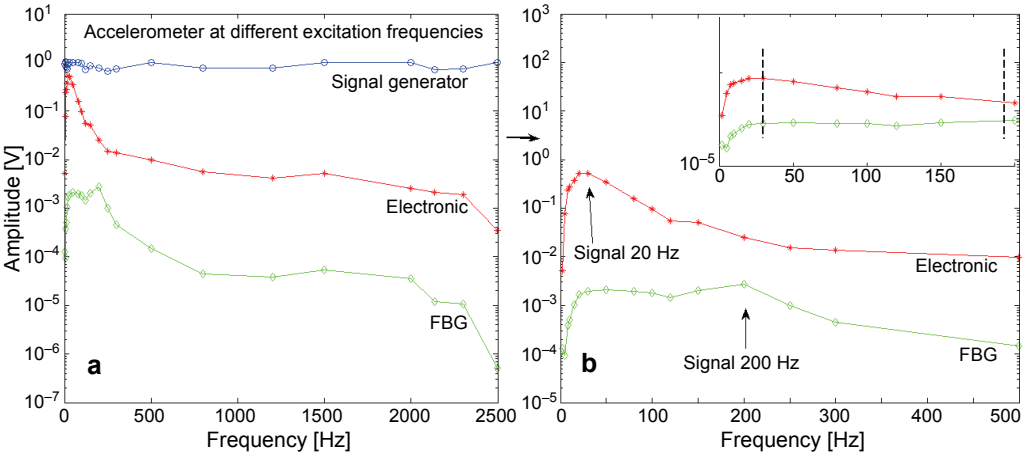

Fig. 5. Signal generator and the accelerometers outputs at different excitation frequencies.

The performance of the experimental transducer has been demonstrated and acceleration induced FBG wavelength changes can be obtained by the IM-DD. To accomplish vector acceleration measurement, a three-axis FBG accelerometer based on the single-axis FBG accelerometer was proposed.

4.2. Three-axis test

A photograph of the three-axis accelerometer is shown in Fig. 6. Three pairs of FBGs were marked as *X*-, *Y*- and *Z*-axis artificially. A proof mass was used to sense acceleration in the *X*-, *Y*-, and *Z*-directions. A series of shaking tests were conducted on each of the sensing axes separately. The responses of other horizontal axes were observed.

The data acquisition was at 10000 samples per second and the sampling number was 20000. Other experimental conditions are the same as the single-axis accelerometer.

In the present study, *Y*-axis was used as the main axis to sense the excitation signals vertically. The presentations of the signals are provided in the following figures.

At 2 Hz, the output of the *Y*-axis (in vertical axis) followed the excited signal in time domain approximately and the outputs of other axes were completely buried by internal noise (Fig. 7**a**). The *Y*-axis response is 1.0776 times (0.65 dB) the *X*-axis and

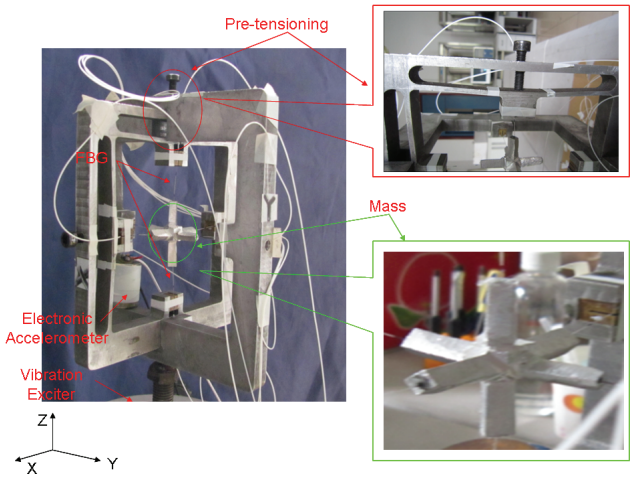

Fig. 6. Photograph of the three-axis accelerometer.

1.0941 times (0.78 dB) the *Z*-axis. It shows the total light intensity that is reflected by the two FBG elements of *Y*-axis is highest. The fundamental frequency component was observed at 2 Hz in *Y*-axis and the signal-to-noise rate is low (Fig. 7**b**).

At 100 Hz, the output of the *Y*-axis more closely followed the excitation signal (Fig. 8**a**) and the amplitude of the output signal was found at around 0.01697 V, which is higher than other horizontal axes. It indicates that the main axis is effective in measuring the exposed acceleration. The fundamental frequency components were

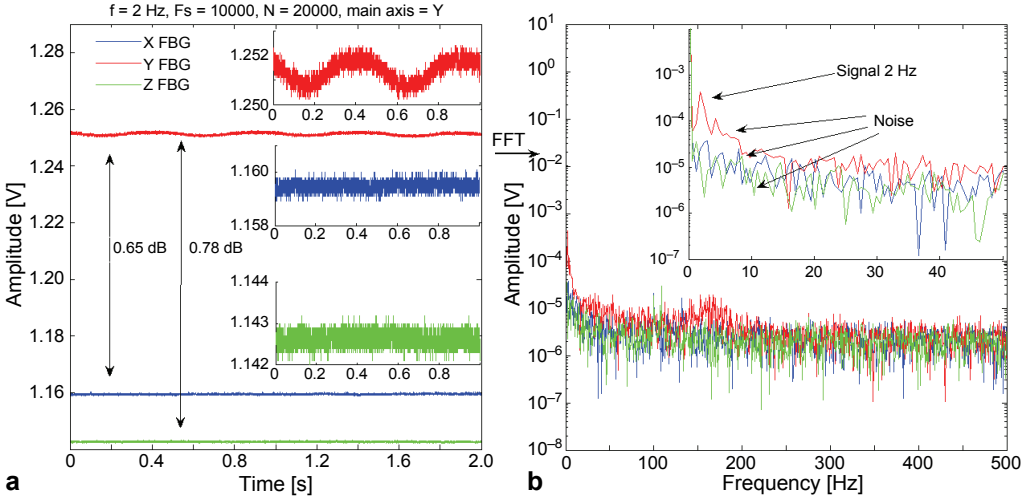

Fig. 7. Output signals of the FBG accelerometer at 2 Hz excitation (**a**); Fourier transform of the signals of the FBG accelerometer (**b**).

observed at 100 Hz in all axes. The *Y*-axis response is 16.97 times (24.6 dB) the *X*-axis and 40.13 times (30.07 dB) the *Z*-axis (Fig. 8**b**). It shows that the transducer is sensitive to a cross-axis response.

The main axis's shaking drove other axes vibration with the same frequency. The cross-axis response is influenced by some factors, such as the geometric properties

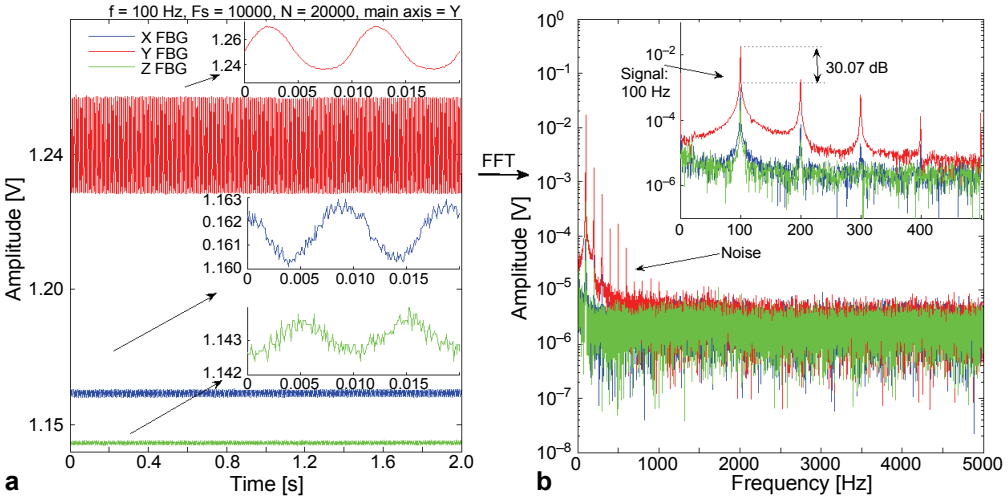

Fig. 8. Output signals of the FBG accelerometer at 100 Hz excitation (**a**); Fourier transform of the signals of the FBG accelerometer (**b**).

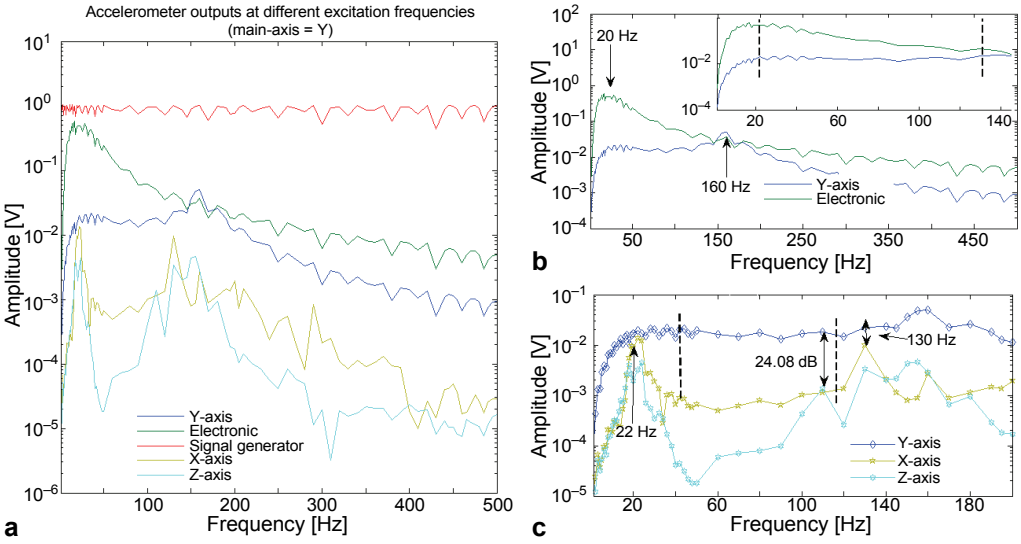

Fig. 9. Signal generator and the accelerometers outputs at different excitation frequencies (**a**); the *Y*-axis of the FBG accelerometer and the electronic outputs at different excitation frequencies (**b**); three axes of the FBG accelerometer outputs at different excitation frequencies (**c**).

of the mass, the mechanical structure, the fabrication, *etc*. To improve the transducer's sensitivity, the mass was decreased from cube to cross-shaped. The fibers were bonded rigidly together at the center of the mass.

The frequency response of *Y*-axis shows similar trends as produced by the electronic accelerometer (Fig. 9**a**). The resonant frequency of the *Y*-axis is 160 Hz, which is higher than the electronic accelerometer. A flat region was observed at lower frequency band (Fig. 9**b**). It indicates that the *Y*-axis does measure the imposed accelerations and has a wide range of measuring acceleration. However, Fig. 9**c** compares the *Y*-axis response with the horizontal axes response. Over the band considered, the *Y*-axis response is approximately 16 times (24.08 dB) horizontal axes, especially at 22 Hz and 130 Hz, indicating it to be sensitive to cross-axis signals.

5. Conclusions

A three-axis accelerometer based FBG is presented in this paper. A novel mechanical pretension was proposed. The IM-DD interrogation technique was adopted to optimize the resolution of detected signals and lower the experiment cost.

Experimental results demonstrate that the accelerometer is meaningful. The natural frequency is 160 Hz obtained from experiment and the suitable measurement frequency range is between 0 and 500 Hz. The SNR of the main axis increases as the excitation frequency increases. However, a flat response with an entire range of vibration frequency was not obtained due to the structure design and the way of fabrication. Multiple harmonics were observed and decreased the resolution of the system. The cross-axis excitation was observed in experiment. The sensitivity of our FBG accelerometer is already comparable to a conventional electronic based accelerometer over some regions of the frequency spectrum. Further improvements can be obtained by a careful design of the sensor geometry and optimization of the acquisition system.

Obtaining acceleration in any spatial direction is the desirable feature for the accelerometer design. The future work will focus on the design of an effective noise reduction technique and minimizing the size of the structure.

Acknowledgments – This work is financially supported by China NCET-10-0541, Independent Innovation Foundation of Shandong University Grant No. 2012ZD015 and China NSFC (No. 51079080).

References

[1] Jones M., *Structural-health monitoring: a sensitive issue*, Nature Photonics **2**(3), 2008, pp. 153–154.

[2] Gagliardi G., Salza M., Avino S., Ferraro P., De Natale P., *Probing the ultimate limit of fiber-optic strain sensing*, Science **330**(6007), 2010, pp. 1081–1084.

[3] Nikles M., Ravet F., *Distributed fibre sensors: depth and sensitivity*, Nature Photonics **4**(7), 2010, pp. 431–432.

[4] Othonos A., Kali K., *Fiber Bragg Gratings, Fundamentals and Applications in Telecommunications and Sensing*, Artech House, Boston, 1999.

[5] DA COSTA ANTUNES P.F., LIMA H.F.T., ET AL., *Optical fiber accelerometer system for structural dynamic monitoring*, IEEE Sensors Journal **9**(11), 2009, pp. 1347–1354.
[6] AU H.Y., KHIJWANIA S.K., TAM H.Y., *Fiber Bragg grating based accelerometer*, Proceedings of SPIE **7004**, 2008, article 70042S.
[7] FENDER A., MACPHERSON W.N., ET AL., *Two-axis temperature-insensitive accelerometer based on multicore fiber Bragg gratings*, IEEE Sensors Journal **8**(7), 2008, pp. 1292–1297.
[8] MITA A., YOKOI I., *Fiber Bragg grating accelerometer for structural health monitoring*, Proceedings of 5th International Conference on Motion and Vibration Control, 2000, p. 1.
[9] TODD M.A., JOHNSON G.A., ALTHOUSE B.A., VOHRA S.T., *Flexural beam based fiber Bragg grating accelerometer*, IEEE Photonics Technology Letters **10**(11), 1998, pp. 1605–1607.
[10] BERKOFF T.A., KERSEY A.D., *Experimental demonstration of a fiber Bragg grating accelerometer*, IEEE Photonics Technology Letters **8**(12), 1996, pp. 1677–1679.
[11] ANTUNES P., VARUM H., ANDRÉ P., *Uniaxial fiber Bragg grating accelerometer system with temperature and cross axis insensitivity*, Measurement **44**(1), 2011, pp. 55–59.
[12] HE S.L., DONG X.Y., ZHANG S.Q., NI K., CHAN C.C., SHUM P., *Temperature-insensitive 2-D fiber Bragg gratings accelerometer*, International Conference on Communications and Mobile Computing, CMC, 2010, pp. 52–55.
[13] MORIKAWA S.R.K., RIBEIRO A.S., REGAZZI R.D., VALENTE L.C.G., BRAGA A.M.B., *Triaxial Bragg grating accelerometer*, Optical Fiber Sensors Conference Technical Digest, OFS, 2002.
[14] MORIKAWA S.R.K., VALENTE L.C.G., NOGUEIRA M.M., BRAGA A.M.B., *Temperature compensated fiber Bragg grating accelerometer*, SEM Annual Conference and Exposition on Experimental and Applied Mechanics, Portland, OR, USA, 2005.
[15] ZENG N., SHI C.Z., ZHANG M., WANG L.W., LIAO Y.B., LAI S.R., *A 3-component fiber-optic accelerometer for well logging*, Optics Communications **234**(1–6),2004, pp. 153–162.
[16] YU F.T. S., SHIZHUO YIN, [EDS.], *Fiber Optic Sensors*, Marcel Dekker, New York, Basel, 2002.
[17] WU N., *Fiber Bragg Grating Based Accelerometer*, Diss. Dalhousie University, Canada, 2009.
[18] MYNBAEV D.K., SCHEINER L.L., *Fiber-Optic Communications Technology*, Prentice Hall, New Jersey, USA, 2001.
[19] KA O. LEE, CHIANG K.S., ZHIHAO CHEN, *Temperature-insensitive fiber-Bragg-grating-based vibration sensor*, Optical Engineering **40**(11), 2001, pp. 2582–2585.

Received February 18, 2012
in revised form June 4, 2012